

Initial NaCl-induced atmospheric corrosion of a dual-phase Cu60-40Zn alloy - Effect of UV illumination

Xiaoying Sun^{1,2}, Zhuoyuan Chen^{1,2,*}, Jiarun Li¹, Jian Hou² and Likun Xu²

¹ Key Laboratory of Marine Environmental Corrosion and Bio-fouling, Institute of Oceanology, Chinese Academy of Sciences, 7 Nanhai Road, Qingdao 266071, China

² State Key Laboratory for Marine Corrosion and Protection, Luoyang Ship Material Research Institute, Wenhai Road, Qingdao 266237, China.

*E-mail: zychen@qdio.ac.cn

Received: 25 March 2018 / Accepted: 22 May 2018 / Published: 5 July 2018

In this paper, the effect of ultraviolet (UV) illumination on the NaCl-induced atmospheric corrosion of a Cu60-40Zn alloy was investigated. UV illumination affects the atmospheric corrosion of the Cu60-40Zn alloy in terms of corrosion rate, corrosion morphology and corrosion products. The NaCl-induced atmospheric corrosion rate of the Cu60-40Zn alloy increases under UV illumination due to the increase of the corrosion initiation sites and the photovoltaic effect of the corrosion products. The increased photoinduced potential and the transfer of the photogenerated electrons from the substrate Cu-Zn alloy to the corrosion products provide evidence for the accelerated anodic reactions under light illumination, and thus promote the atmospheric corrosion of the Cu60-40Zn alloy under UV illumination.

Keywords: Cu-Zn alloy; atmospheric corrosion; UV illumination; NaCl particles; XPS

1. INTRODUCTION

The Cu-Zn alloy (brass) is extensively utilized in petroleum refineries, refrigeration, chemical plants and marine engineering due to its superior electrical and thermal conductivities, good corrosion resistance, and desirable hardness and strength compared to pure copper [1]. Nonetheless, the brass suffers from appreciable atmospheric corrosion when exposed to the dry and wet cycle environments containing chloride ions. To this end, extensive investigations have been conducted to clarify the mechanism of marine atmospheric corrosion of brass [2-7].

Brass is divided into two types. One is α brass, and it is a single phase alloy with the concentration of zinc less than 35 wt%. The other one is the duplex brass, which is comprised of α -phase and β -phase and whose concentration of zinc is 35-45 wt%. The Cu-Zn alloys containing zinc

more than 15 wt% are predisposed to undergo a dealloying process by selective removal of zinc, named dezincification, which often occurs during the atmospheric exposure [8-11]. Therefore, Zn concentration can affect the corrosion type of the Cu-Zn alloys in atmospheric environment. Herman and Castillo studied a short-term atmospheric corrosion of various copper-based alloys in natural environment [12]. Plug type dezincification of Cu70-30Zn brass at all exposure locations and pitting corrosion coupled with plug type dezincification of Cu56-25Zn at the industrial and industrial marine sites were observed. Barr and Hackenberg investigated the corrosion products of α brass (20~35 wt% Zn) using XPS and the results reflected that a relatively thick zinc oxide (ZnO) layer initially formed on α brass at room temperature with the relative humidity (RH) of 35 %, above which a thin layer of cupric oxide (CuO) was detected and the outermost thin film was composed of CuO and Cu(OH)₂ [13]. When it is exposed to chloride-containing solutions, brass forms a surface film consisting of a mixture of ZnO, Cu₂O and CuO, wherein the molar ratios among the oxides depend on pH, chloride ion concentration and Zn content of the brass [14]. An overwhelming majority of the brass surface was covered with amorphous zinc hydroxyl carbonate (Zn₅(CO₃)₂(OH)₆) and ZnO after exposure in sites with low chloride deposition rates [8].

Solar illumination does have influence on metals exposed to atmospheric environments [15, 16], nonetheless, there are few reports focused on the effect of solar illumination on the atmospheric corrosion of brass. Lin and Frankel studied the atmospheric corrosion of NaCl particles deposited copper with UV illumination under CO₂ atmosphere, and found that UV has a strong promotion effect on the formation of cuprite due to the interactions between UV photons and cuprite [17]. Chen et al. reported that UV illumination decomposes molecular oxygen to atomic oxygen, which directly participates in the oxidation of silver exposed in the atmospheric environment [18]. Recently, a work on chloride-containing atmospheric corrosion of Cu40Zn by Zhang et al. verified the presence of hydrozincite (Zn₅(CO₃)₂(OH)₆), simonkolleite (Zn₅(OH)₈Cl₂·H₂O), and small amounts of CuO, Cu₂O, ZnO in the corrosion products formed at 70% RH humidified air containing 1000 ppm of CO₂ [19]. It has been reported that Cu₂O [20-24], CuO [21, 22], and ZnO [25, 26] have semiconductor properties and they will produce photogenerated electrons and holes under light illumination. These photogenerated charge carriers can influence the cathodic and anodic reactions, and thus affect the atmospheric corrosion of the metallic substrate. However, the investigation on the specific influence mechanism of light illumination on the atmospheric corrosion of brass is quite scarce to date. In this paper, a quantitative study of the role of UV illumination on the NaCl-induced atmospheric corrosion of a Cu60-40Zn alloy was performed. Microgravimetry, scanning electron microscopy (SEM), Fourier transform infrared (FT-IR) spectroscopy, X-ray photoelectric spectroscopy (XPS) and electrochemical tests were further applied to identify the corrosion processes and the corrosion products after 1, 2 and 4 weeks of laboratory exposure to humidified pure air.

2. EXPERIMENTAL

2.1 Sample preparation

The material investigated in this study was a commercial Cu60-40Zn alloy. The as-received sheets were of 1mm in thickness. The chemical composition of this alloy is given as follows (wt%):

61.3700 Cu, 0.0025 P, 0.0062 Pb, 0.0060 Fe, and balance Zn. The microstructure of the Cu60-40Zn alloy is demonstrated in Figure 1. The dual-phase structure comprised of α phase and β phase can be clearly distinguished in a SEM image after slighted etching for 20 s in the solution containing $\text{NH}_3\cdot\text{H}_2\text{O}$ (100 mL), H_2O_2 (40 mL) and H_2O (100 mL). The irregular shaped β phase with the typical size ranging from 10 to 20 μm contains more Zn compared with α phase, and it is embedded in the α phase after etching [27, 28].

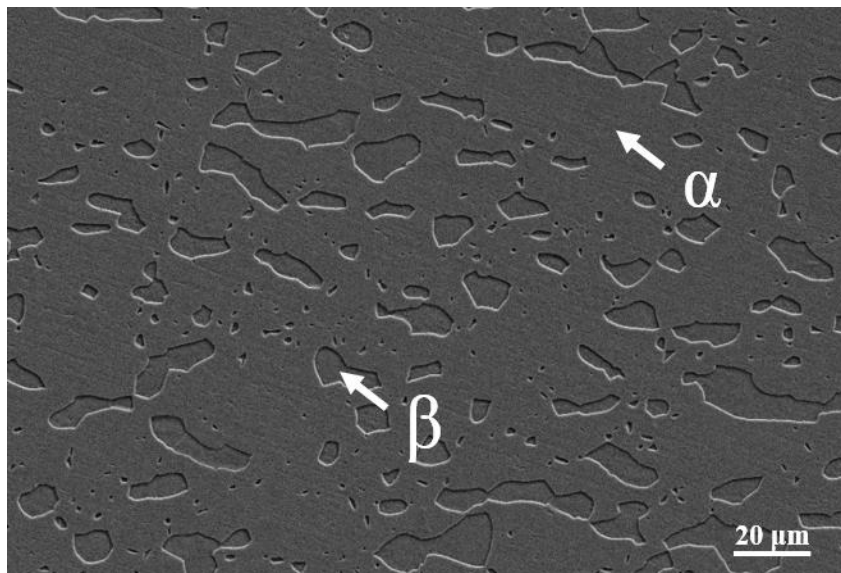


Figure 1. Dual-phase microstructure of the as-received Cu60-40Zn alloy revealed by SEM after etching.

Prior to the laboratory exposure, each specimen ($50\times 10\times 1$ mm) was ground down to 3000-grit using SiC paper and then polished with diamond paste down to 0.5 μm . Subsequently, the specimens were wiped with absorbent cotton, and ultrasonically cleaned in acetone of analytical grade for 5 minutes. After that, the prepared specimens of the Cu60-40Zn alloy were stored in a desiccator over silica gel for approximately 24 hours before exposure. In this study, $15\ \mu\text{g}\cdot\text{cm}^{-2}$ of NaCl particles were evenly deposited on the surface of each specimen by uniformly transferring an appropriate amount of NaCl saturated ethanol of analytical grade, and the total amount of deposited NaCl can be determined by gravimetric method after ethanol volatilization [29].

2.2 Laboratory exposure

The Cu60-40Zn alloy specimens were exposed in a rectangular glass chamber ($50\times 40\times 30$ cm) whose thickness of the glass was 5 mm. A glass shelf with many perforated small holes was placed inside the exposure chamber, and the exposure chamber was divided into two parts. In the lower part of the glass chamber, saturated K_2SO_4 solution was adopted to keep the RH at 97%; whilst the Cu60-40Zn alloy specimens were exposed in the upper part. During the laboratory exposure, a glass shelf on which two glass blocks with different heights were fixed by glue to tilt the Cu60-40Zn alloy specimens approximately 15° from horizontal.

Additionally, two 9 W quartz UV lamps (T8, Shanghai Sitong Co. Ltd., Shanghai, China) with an optical intensity of $0.538 \text{ mW}\cdot\text{cm}^{-2}$ were installed on the top of the glass cover as the UV light source in the chamber. The wavelength of the light generated by the UV lamps is of 220 ~ 300 nm, and about 90% of the energy was contributed by the light in 253.7 nm wavelength. The external surfaces of the chamber were covered with black tapes to prevent the UV light from penetration.

An air pump was adopted to provide pure airflow to pass through the exposure chamber with a velocity of $30 \text{ mL}\cdot\text{min}^{-1}$, which was accurately controlled by a mass flow controller. Prior to passing through the exposure chamber, the flowing air was bubbled in a saturated K_2SO_4 solution and subsequently passed through two empty bottles. Except for the air pump, the whole exposure system was located in a thermostat (HWS, Dongnan Co. Ltd., Ningbo, China) in which the exposure temperature was controlled at $25\pm 1 \text{ }^\circ\text{C}$. More details of the apparatus for the atmospheric exposure were reported in our previous work [30]. All specimens were exposed in humidified air at 97% RH and $25 \text{ }^\circ\text{C}$ for 1, 2 and 4 weeks in the dark or under UV illumination. The RH was monitored by a temperature/humidity sensor (XMTA-2001, Yaoaote Instrument Co. Ltd., Dongguan, China). Nine parallel specimens were used for each exposure condition. Each test was repeated three times in order to ensure reproducibility of the measurements.

2.3 Mass gain and mass loss measurements

After laboratory exposure, the corrosion effect on the Cu60-40Zn alloy was quantitatively determined by measuring the increase and decrease in weights of the specimens. Mass gain equals to the mass of specimens after exposure minus that before the exposure with deposited NaCl particles; Mass loss equals to the original mass of specimen (without deposited NaCl particles) minus the mass after removal of the corrosion products. A microbalance (Sartorius CPA 26P, Germany) with a $\pm 4 \text{ }\mu\text{g}$ -specified precision ($\pm 0.4 \text{ }\mu\text{g}\cdot\text{cm}^{-2}$ in this study) was adopted. Additionally, a stainless steel as a reference sample was weighed to eliminate the system error of the microbalance during the weight measurement. According to ISO standard [31], the corrosion products formed on the Cu60-40Zn alloy surface after laboratory exposure were removed by ultrasonically pickling the samples in a mixed solution by dissolving 50 g amidosulfonic acid (sulfamic acid) into distilled water to form a 1000 mL solution. Triplicate specimens were taken for the measurements of the mass gains and mass losses after laboratory exposure at different conditions.

2.4 Characterization of corrosion products

The corrosion products after laboratory exposure were identified by FT-IR spectroscopy (Nicolet IS10 infrared spectrophotometer, USA) with a MCT detector ($4000 \sim 400 \text{ cm}^{-1}$). FT-IR spectra were obtained in the transmission mode by adding 128 interferograms with a resolution of 4 cm^{-1} using the KBr pellet method. The corrosion morphologies after laboratory exposure were analyzed by a SEM (S-3400N Scanning Electron Microscope, Hitachi, Tokyo, Japan). X-ray photoelectron spectroscopy (XPS) tests were performed on an ESCALAB 250Xi (Thermo Fisher Scientific) spectrometer using a monochromatized Al Ka ($h\nu=1486.6 \text{ eV}$) source. Energy calibration

was based on C 1s 284.8 eV. Sputtering etching of the corroded Cu60-40Zn alloy after 1 week of exposure with Ar gas was employed to study the corrosion products beneath the surface layer with an etching speed of 0.2 nm/s.

2.5 Photoelectrochemical/electrochemical performance measurements

In order to clarify the photoelectrochemical/electrochemical performance, the corrosion products formed on the Cu60-40Zn alloy after laboratory exposure were peeled off and the corrosion product thin-film (CPTF) electrode was prepared by evenly depositing them onto the surface of fluorine-doped tin-oxide (FTO) conductive glasses. Because the corrosion products are insoluble, and the FTO conductive glass merely plays a role of a conductor, therefore, the CPTF electrode could be relatively stable in electrolyte solutions. Moreover, this method of manufacturing CPTF electrode has been applied in the field of photocatalysis [32, 33]. The FTO conductive glass was of 13×10×1 mm in size. Prior to the deposition, the FTO glass was ultrasonically cleaned in acetone for 5 min, subsequently rinsed by deionized water and dried with a clean dry airflow. A copper wire was connected to the conductive side of the FTO glass by silver paste, and then sealed with silicone rubber, leaving a 1-cm² working area for depositing the corrosion products. The as-prepared corrosion products of the Cu60-40Zn alloy were mixed with deionized water in an agate mortar and then ground for 10 min to form a slurry, which was evenly distributed onto the working area of the FTO glass consequently.

Mott-Schottky plots were measured by Parstat 4000+ Electrochemical Workstation (AMETEK, Inc, Princeton, USA) in the dark, which employed a 10 mV AC perturbation signal at a constant frequency of 1 kHz with a variable potential from -0.2 to 0 V versus Ag/AgCl (saturated KCl) reference in a three-electrode cell system. A CPTF electrode acted as the working electrode, a platinum foil performed as the counter electrode and an Ag/AgCl (saturated KCl) electrode served as the reference electrode, respectively.

Photoelectrochemical performance measurements including photoinduced potential and photoinduced current density were carried out in 5.2 wt% NaCl solution using CHI660D Electrochemical Workstation (Shanghai Chenhua Instrument Co. Ltd., Shanghai, China) under intermittent white light illumination. The 5.2 wt% NaCl solution was adopted because the deposited NaCl particles on the specimen surface would absorb moisture from the ambient environment to form an electrolyte layer in which the NaCl concentration is 5.2 wt% at 97% RH and 25 °C [34]. The white light source was a 300-W Xe arc lamp (PLS-SXE300, Beijing Changtuo Co. Ltd., Beijing, China), and the wavelength of generated light was 100~2000 nm with a power energy density of 320 mW·cm⁻². During the photoelectrochemical performance measurements, a flat circular quartz window in 30 mm diameter was installed on one side of the cell to pass through light for illuminating on the CPTF electrode. A two-electrode system comprised of a CPTF electrode as the working electrode and an Ag/AgCl (saturated KCl) electrode as the reference electrode was applied for measuring the photoinduced potential. Besides, the photoinduced current densities generated by the corrosion products under white light illumination were measured without any polarization using the CHI 660D Electrochemical Workstation [30, 35-37].

3. RESULTS AND DISCUSSION

3.1. Characterization of corrosion rates

Figure 2 shows the mass gains and mass losses of the Cu60-40Zn alloy pre-deposited with $15 \mu\text{g}\cdot\text{cm}^{-2}$ NaCl particles after 1, 2, and 4 weeks of exposure in 97% RH humidified pure air at 25°C in the absence and presence of UV illumination. As shown in Figure 2, the mass gains and mass losses increase with increasing the exposure time. In addition, the mass gains and mass losses obtained under UV illumination are larger than those obtained in the dark after identical exposure duration. However, an exception presents at 1 week of exposure as depicted in Figure 2b, in which the mass loss of UV illuminated specimens is slightly less than that of the specimen in the dark. The amount of the formed corrosion products after 1 week of exposure is comparatively less, leading to a weak effect of UV illumination on the atmospheric corrosion of the Cu60-40Zn alloy in comparison with those experiencing 2 and 4 weeks of exposure.

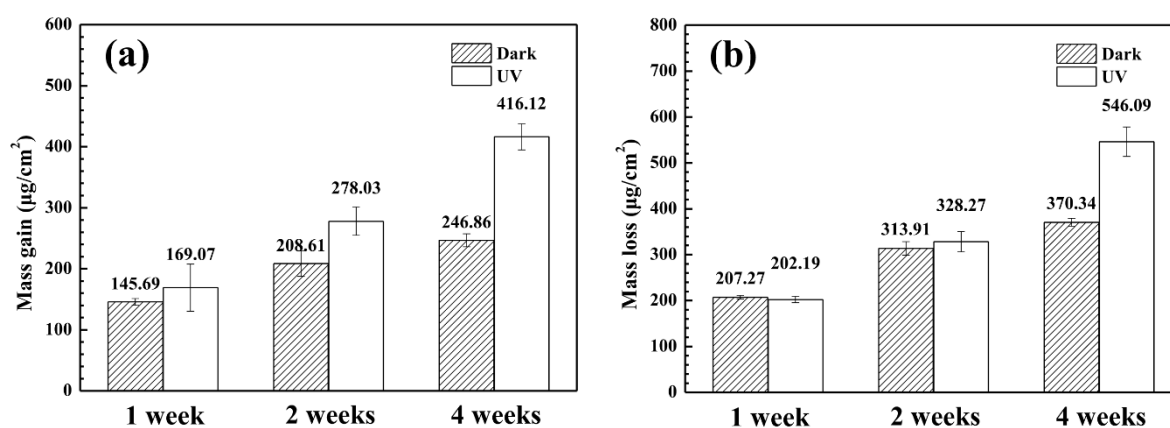


Figure 1. (a) Mass gains and (b) mass losses of the Cu60-40Zn alloy pre-deposited with $15 \mu\text{g}\cdot\text{cm}^{-2}$ NaCl particles after 1, 2, and 4 weeks of exposure in 97% RH humidified pure air at 25°C in the absence and presence of UV illumination.

3.2 Characterization of the corrosion morphologies after exposure

The surface morphologies of the Cu60-40Zn alloy after exposure at different conditions were studied using SEM, and the relevant results are shown in Figure 3. After 1, 2 and 4 weeks of exposure in the dark, granular crystals are the major characteristic in the center of the observed areas, such as zones A, C and E in Figures 3a, 3b and 3c, respectively. Whereas the needle-like crystals present in the vicinity of the observed areas as shown in zones B, D, and F in Figures 3a, 3b and 3c, respectively. The visual feature characterized by voluminous and tenacious deposits is a reminiscence of a meringue dessert topping associated with dezincification [9]. The meringue deposition is a typical dezincification on brass components, along with plug dezincification [9]. The heterogeneous surface exhibiting different morphologies including granular and needle-like crystals is probably due to the difference of the local potential and chemistry among the spreading areas. In the context of deliquescence, the initially deposited NaCl tends to retain as discrete droplets on the surface; and then these droplets

spread out associated with forming continuous NaCl-containing aqueous films. It has been reported that the initial NaCl concentrated areas are comparatively anodes with lower pH and higher chloride concentration to the peripheral spreading areas which are regarded as cathodes with higher local pH and lower chloride content [38]. In the condition of the NaCl-induced atmospheric corrosion of Zn, simonkolleite ($Zn_5(OH)_8Cl_2 \cdot H_2O$) is expected to be formed in the central anodic area, and hydrozincite ($Zn_5(CO_3)_2(OH)_6$), is expected to be formed preferentially in the more peripheral cathodic area [39, 40]. Furthermore, both the density and the thickness of granular and needle-like crystals are promoted with increasing the exposure time.

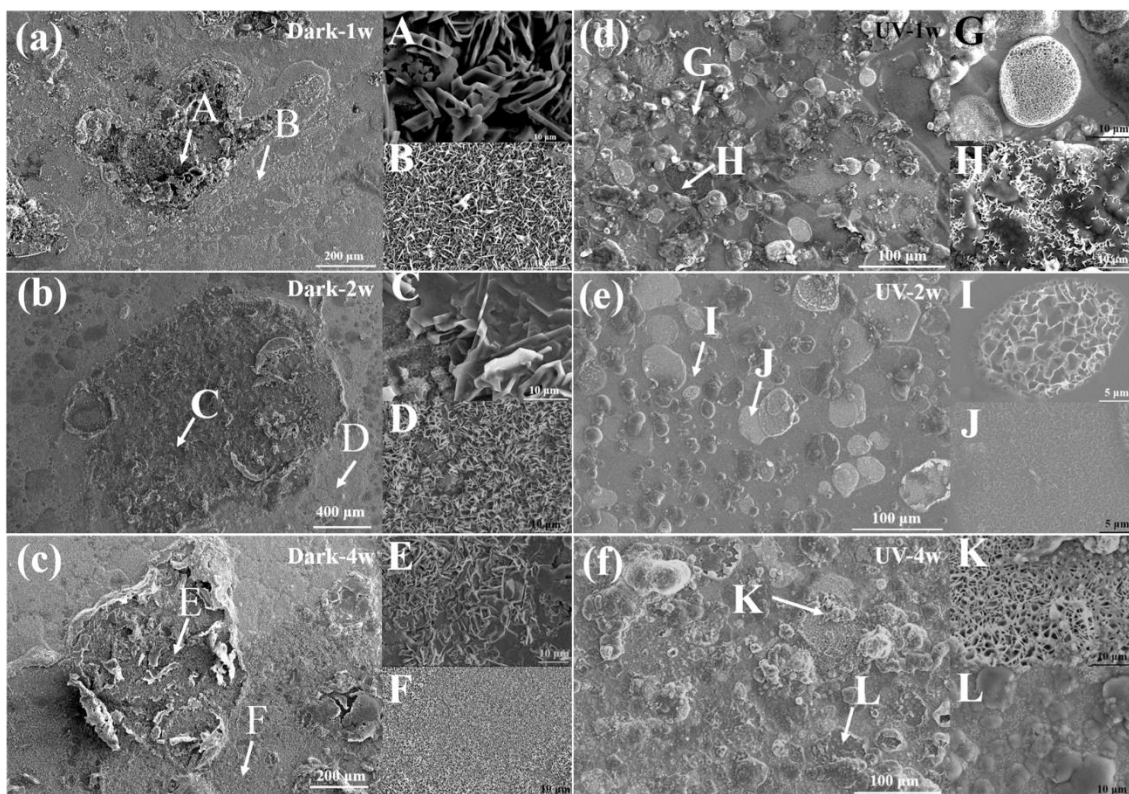


Figure 2. SEM images of the Cu60-40Zn alloy pre-deposited with $15 \mu\text{g}\cdot\text{cm}^{-2}$ NaCl particles after 1 (a), 2 (b), 4 (c) weeks of exposure in the dark and after 1 (d), 2 (e), 4 (f) weeks of exposure under UV illumination.

Unlike the corroded morphologies in the dark, the morphologies of UV illumination embody striking difference identified by small islands distributing widely on the surface (Figures 3d-3f), elucidating a promoted corrosion under UV illumination. There are two types of islands observed in the corrosion products. One is characterized as porous microstructure as shown in zones G, I and K in Figures 3d, 3e and 3f, respectively. This porous microstructure is probably arisen from Zn-rich β phases, because these small porous islands with layered structures were observed previously and its composition corresponded quantitatively to that of simonkolleite [41]. The micro-cracks in porous islands could act as transmission channels for oxygen and electrolyte to penetrate into and get contacted with matrix, by which the atmospheric corrosion under UV illumination would be promoted [39, 40]. Besides, the porous islands change less in microstructure with increasing exposure time,

except for their size. The other type of islands is covered with whiskers (zones H, J, and L), which distribute discretely after 1 week of UV illumination. Nonetheless, they perform consecutively after 2 weeks of exposure, and finally form fluffy balls over 4 weeks of exposure. After exposed under UV illumination for 4 weeks (Figure 3f), the entire surface of the specimen was covered with corrosion products validating that there were more corrosion initiation sites under UV illumination than those in the dark.

3.3 Characterization of corrosion products using FT-IR spectroscopy

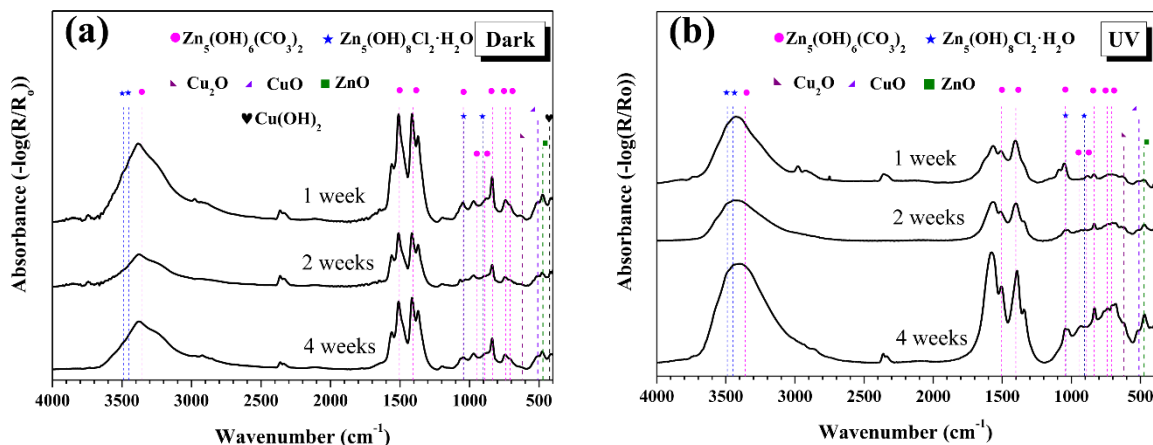


Figure 3. FT-IR absorbance spectra of the Cu60-40Zn alloy pre-deposited with $15 \mu\text{g}\cdot\text{cm}^{-2}$ NaCl and exposed for 1, 2, and 4 weeks in humid pure air with 97% RH at $25 \text{ }^\circ\text{C}$ in (a) the absence and (b) presence of UV illumination.

To get more detailed information, the corrosion products formed after exposure were characterized using FT-IR spectroscopy. Figure 4 displays the typical spectra of the corrosion products formed on the Cu60-40Zn alloy after 1, 2, and 4 weeks of exposure in humid pure air with 97% RH at $25 \text{ }^\circ\text{C}$ in the absence and presence of UV illumination. The corrosion products under UV illumination are composed of simonkolleite ($\text{Zn}_5(\text{OH})_8\text{Cl}_2\cdot\text{H}_2\text{O}$), hydrozincite ($\text{Zn}_5(\text{OH})_6(\text{CO}_3)_2$), zinc oxide (ZnO), cuprite (Cu_2O), and cupric oxide (CuO). Apart from the aforementioned corrosion products, copper hydroxide ($\text{Cu}(\text{OH})_2$) is also detected in the corrosion products formed in the dark. As shown in Figure 4, the broad band at 3360 cm^{-1} is attributed to H-OH stretching, and another OH vibration is -OH stretching at 890 cm^{-1} . Metal hydroxide deformation is presented at 945 cm^{-1} . The internal vibration assignments for carbonate are at 1045 cm^{-1} for ν_1 ; 835 cm^{-1} for ν_2 ; $\sim 1390 \text{ cm}^{-1}$ and 1505 cm^{-1} for ν_3 ; and 707 cm^{-1} and 738 cm^{-1} for ν_4 , respectively. Components of these spectra mentioned above appropriately match the zinc hydroxycarbonate complex molecule of $\text{Zn}_5(\text{OH})_6(\text{CO}_3)_2$, which are also consistent with previous infrared reflection absorption spectroscopy (IRAS) analyses [19, 42-45]. $\text{Zn}_5(\text{OH})_8\text{Cl}_2\cdot\text{H}_2\text{O}$ has an analogous structure to $\text{Zn}_5(\text{OH})_6(\text{CO}_3)_2$, however, chloride ions are bound to the zinc atoms and hydroxide groups. Comparing to $\text{Zn}_5(\text{OH})_6(\text{CO}_3)_2$, the chloride ion in $\text{Zn}_5(\text{OH})_8\text{Cl}_2\cdot\text{H}_2\text{O}$ causes the shift in metal hydroxide deformation and hydroxide stretching [46]. In detail, the bands resolved at 3490 cm^{-1} and 3450 cm^{-1} are due to the hydroxyl vibrations from $\text{Zn}_5(\text{OH})_8\text{Cl}_2\cdot\text{H}_2\text{O}$ [42, 43]; metal hydroxide deformations present at 905 cm^{-1} and 720 cm^{-1} are

assigned to the Zn-O-H vibrations from $\text{Zn}_5(\text{OH})_8\text{Cl}_2 \cdot \text{H}_2\text{O}$ [42-44]. Apart from simonkolleite and hydrozincite, zinc oxide with the absorbance at 472 cm^{-1} corresponds to the Zn-O vibration from ZnO [42, 43]. In addition, the bands at 620 cm^{-1} [47-49] and 510 cm^{-1} [47] are from the vibrations from the cuprous oxide and cupric oxide. And, the band at 424.2 cm^{-1} can be assigned to Cu-O stretching mode from $\text{Cu}(\text{OH})_2$ [50, 51].

3.4 Surface corrosion products analyses by XPS

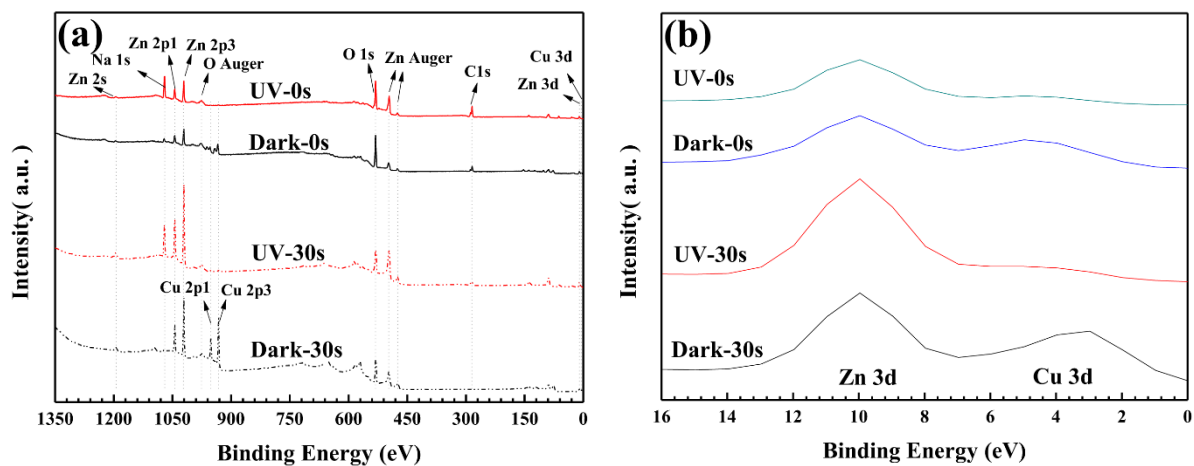


Figure 4. XPS spectra of the Cu60-40Zn alloy (a) after 1 week of exposure in the absence and presence of UV illumination and (b) corresponding Zn 3d and Cu 3d spectra. (0 s: XPS spectra without sputtering; 30 s: XPS spectra after sputter etching for 30 s)

The resolution of FT-IR spectroscopy using the KBr pellet method has a limitation on identifying the corrosion products when taking into account of the UV illumination penetration depth [52], thereby, further XPS analysis of the corrosion products on the surface and the shallow layer (approximate 6 nm beneath the surface by sputtering the corrosion products with Ar gas for 30 s with an etching speed of 0.2 nm/s) after 1 week of exposure in the absence and presence of UV illumination was conducted, and the relevant results are shown in Figure 5. As shown in Figure 5a, the UV illumination resulted in a decrease of both Cu 2p1 and Cu 2p3 signals. Moreover, for the samples exposed in the dark, it is clearly shown that the Cu 2p1 and Cu 2p3 spectra of the shallow layer (Dark-30 s) are more conspicuous than those in the surface (Dark-0 s). Specifically, the atomic percentages of Cu in the corrosion products in the surface detected by XPS in the presence and absence of UV illumination are 0.929% and 9.347%, respectively. Whilst the respective atomic percentages of Cu strikingly increase to 1.535% and 20.064% after 30-s sputtering etching. The spectra of Zn 2p1 and Zn 2p3 can be detected in all cases. These aforementioned results indicate that more Cu-containing products preferred to generate in the dark. However, UV illumination, to a certain extent, promotes the dezincification of Zn due to the increased peak intensities of Zn 2p1 and Zn 2p3 derived from the corrosion products in the presence of UV illumination. In practical, detailed researches have been

carried out on the shifts and width variations in the Zn 3d and Cu 3d lines to determine oxide species [13]. In the present study, the Zn 3d and Cu 3d spectra are introduced in purpose of clarifying whether the corrosion species of Zn and Cu change with depth. In Figure 5b, the peak at 9.9 eV can be attributed to Zn 3d. Furthermore, there is no shift of this peak, elucidating that the Zn-containing corrosion products are the same in spite of depth and UV illumination variations. Under UV illumination, it seems that there was no peak associated with Cu 3d in the context of spectra obtained after sputtering for 0 s and 30 s, which means that the Cu is corroded insignificantly after 1 week of exposure under UV illumination, and this is in agreement with the XPS survey spectra of Cu 2p1 and Cu 2p3 in Figure 5a. Besides, the Cu-containing corrosion products in the dark have changed as shown in Figure 5b, validating by a variation of Cu 3d peak from 5.0 eV in the surface to 2.9 eV in the shallow layer.

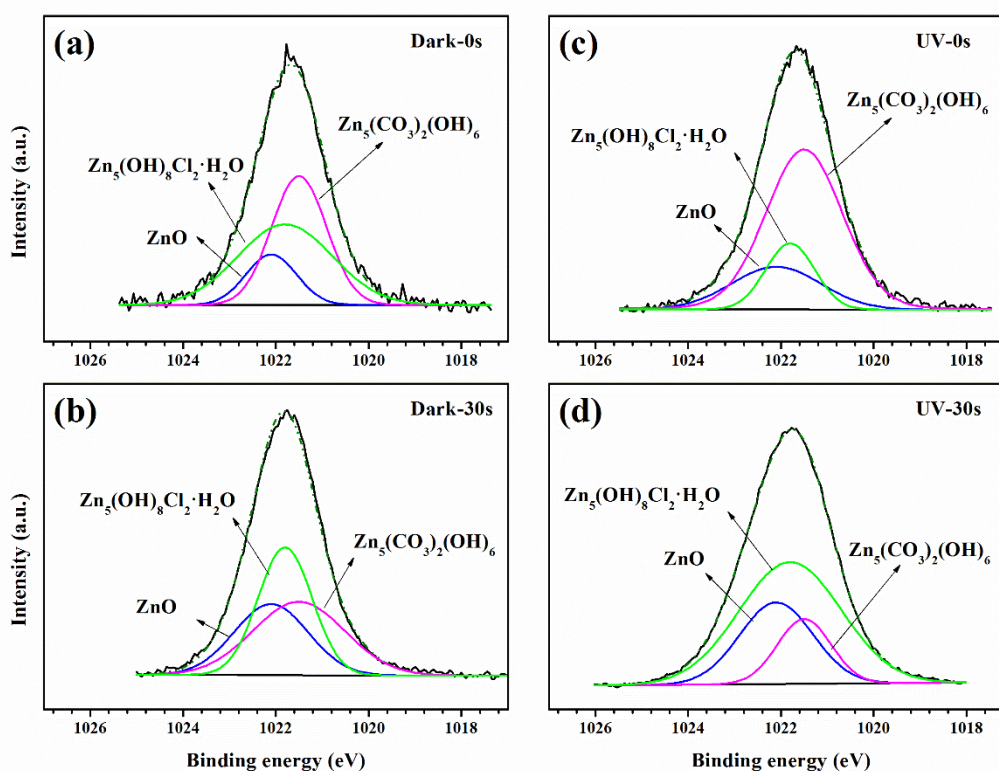


Figure 6. Zn 2p3 high-resolution spectra of the Cu60-40Zn alloy after 1 week of exposure in humid pure air with 97% RH at 25 °C. (a) in the dark without sputtering; (b) in the dark after sputtering for 30 s; (c) under UV illumination without sputtering; (d) under UV illumination after sputtering for 30 s.

In the interest of the specific corrosion species, Cu 2p3 as well as Zn 2p3 high-resolution spectra in the surface and the shallow layer of the corrosion products formed on the Cu60-40Zn alloy after 1 week of exposure in humid pure air with 97% RH at 25 °C were analyzed, and the results are shown in Figures 6 and 7. All the spectra of Zn 2p3 (Figure 6) can be fitted to three components: the first at 1021.5 eV is attributed to the presence of hydrozincite ($Zn_5(OH)_6(CO_3)_2$) [53]; the second at 1021.8 eV is associated with the presence of simonkolleite ($Zn_5(OH)_8Cl_2 \cdot H_2O$) [53, 54]; and the third at 1022.1 eV corresponds to zinc oxide (ZnO) [20, 55]. The analyses of the Zn 2p3 spectra manifest

that the Zn-containing corrosion products are identical despite of UV illumination, which is consistent with the preceding Zn 3d spectra in Figure 5b.

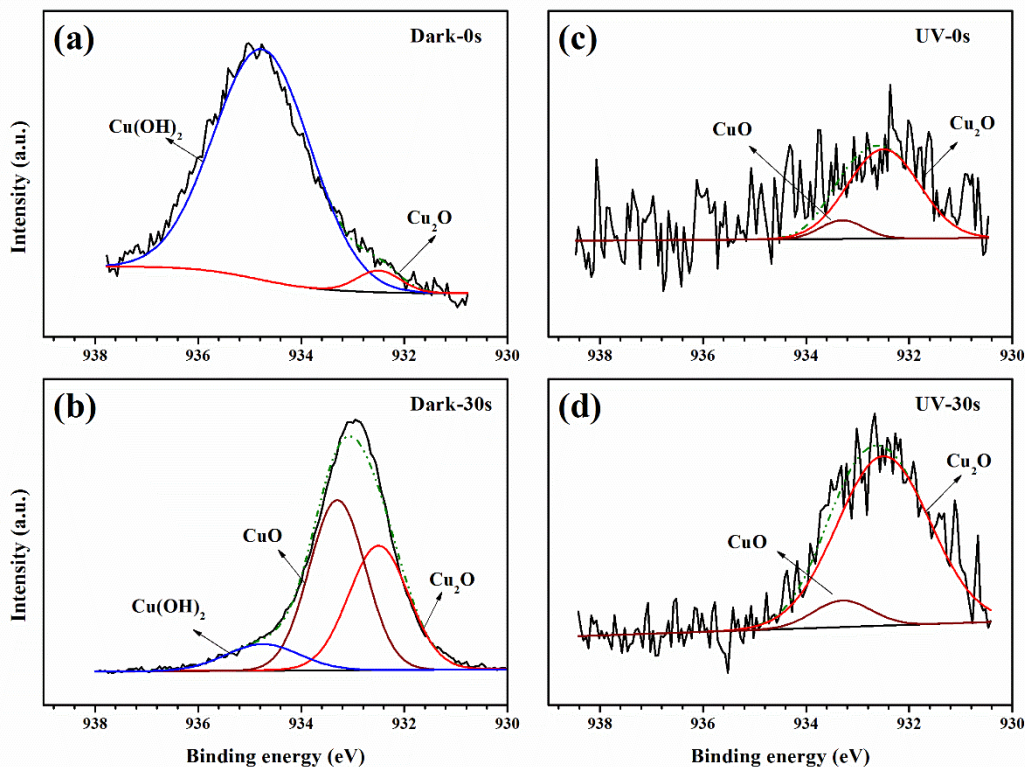


Figure 7. Cu 2p3 high-resolution spectra of the Cu60-40Zn alloy after 1 week of exposure in humid pure air with 97% RH at 25 °C. (a) in the dark without sputtering; (b) in the dark after sputtering for 30 s; (c) under UV illumination without sputtering; (d) under UV illumination after sputtering for 30 s.

Figure 7 compares the Cu 2p3 XPS spectra of the corrosion products on the surface and in the shallow layer after 1 week of exposure in the dark (Figures 7a, 7b) with those obtained after 1 week of exposure under UV illumination (Figures 7c, 7d). It is interesting to note that the Cu 2p3 spectra vary a lot under UV illumination compared to those in the dark. From the curve-resolved Cu 2p3 spectra (Figures 7a, 7b), a contribution from cupric hydroxide ($\text{Cu}(\text{OH})_2$) at 934.75 eV [13] and cuprite (Cu_2O) at 932.5 eV [20, 55, 56] are determined after 1 week of exposure in the dark. The difference of corrosion products formed in the dark from those under UV illumination is that the cupric oxide (CuO) with a binding energy of 933.3 eV [57] merely presents in the shallow layer (Figure 7b) rather than that on the surface (Figure 7a). A previous research on oxidation of the Cu-Zn alloy validated that a relatively thick ZnO layer formed at first, followed by a thin layer of Cu_2O , on which a terminal very thin film of CuO and $\text{Cu}(\text{OH})_2$ was generated finally [13]. This result consists with the corrosion products analysis in this study, i.e., the Cu_2O , CuO and $\text{Cu}(\text{OH})_2$ present in the shallow layer and Cu_2O , $\text{Cu}(\text{OH})_2$ exist on the surface after 1 week of exposure in the dark. The aforementioned spectral characteristics were applied to identify the Cu-containing corrosion products under UV illumination. The binding energy peaks of 932.5 and 933.3 eV respectively imply the presence of Cu_2O and CuO (Figures 7c, 7d), and absence of $\text{Cu}(\text{OH})_2$ in comparison with those in the dark.

3.5 Mott-Schottky analysis

The semiconductor properties of the corrosion products formed after 1, 2 and 4 weeks of laboratory exposure after 1, 2 and 4 weeks were analyzed using Mott-Schottky method, and the relevant results are presented in Figure 8. Positive slopes in Figure 8 indicate that the corrosion products have photoelectric rectifying characteristics similar to n-type semiconductor. According to the XPS results in this study, semiconductor products including ZnO, Cu₂O and CuO were formed. ZnO is a wide bandgap semiconductor and typically has n-type conductivity [20, 58, 59]. Lin et al. reported that the acceleration effect of UV on atmospheric corrosion of Cu was due to the n-type cuprite which can give rise to anodic photocurrent and consequently increase the corrosion rate [60]. It is probable that these n-type corrosion products on Cu60-40Zn in this study cause the acceleration of atmospheric corrosion under UV illumination. Therefore, it is necessary to clarify the photovoltaic effect of the corrosion products formed on the Cu60-40Zn alloy specimens. Moreover, UV illumination doesn't change the electric properties of corrosion products. Since the corrosion products are a complex mixture of semiconductors including Cu₂O, CuO and ZnO, it's difficult to quantitatively identify the amount of each species. For this reason, the Mott-Schottky curves were not applied to further analysis, such as the carrier density and the flatband potential.

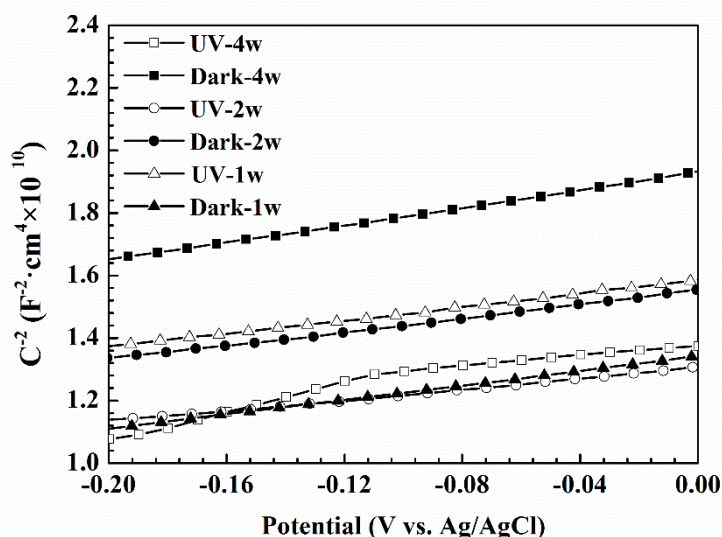


Figure 8. Mott-Schottky plots of the CPTF electrodes in 5.2 wt% NaCl solution tested in the dark. The UV-1w, UV-2w and UV-4w represent the CPTF electrodes made from corrosion products after 1, 2 and 4 weeks of exposure under UV illumination, respectively; the Dark-1w, Dark-2w and Dark-4w stand for CPTF electrodes made from corrosion products after 1, 2 and 4 weeks of exposure in the dark, respectively.

3.6 Analysis of the photovoltaic effect of the corrosion products

To clarify the photovoltaic effect of the corrosion products formed on the Cu60-40Zn alloy after 1, 2 and 4 weeks of exposure to humid pure air with 97% RH at 25 °C under UV illumination, the variations of open circuit potentials (OCPs) of the CPTF electrodes made from the corrosion products after exposure at different conditions were measured as well as the variations of the galvanic current

densities between CPTF electrodes and the Cu60-40Zn alloy under intermittent white light illumination. The results are shown in Figures 9 and 10.

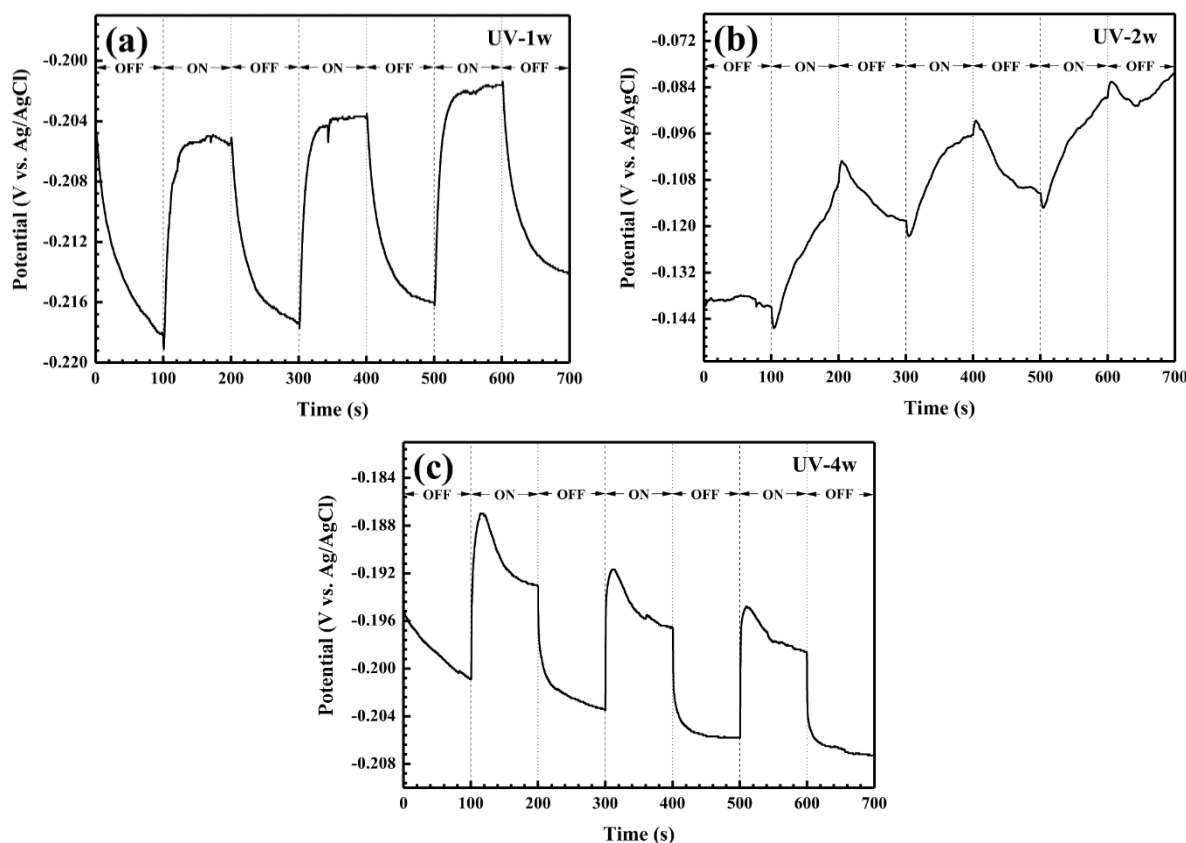


Figure 9. The variations of the OCPs (vs. Ag/AgCl) of CPTF electrodes in 5.2 wt% NaCl solution under intermittent white light illumination. The CPTF electrodes were made from corrosion specimens after 1 (a), 2 (b) and 4 (c) weeks of exposure under UV illumination in humid pure air with 97% RH at 25 °C.

After switching on the white light, the OCPs of the CPTF electrodes made from the corrosion products formed under UV illumination perform a swift positive shift; on the contrary, the OCPs of the CPTF electrodes give an immediate negative shift as soon as the white light was shut off (Figure 9). The potential difference obtained by subtracting the stable OCPs of CPTF electrodes in the dark from that under light illumination, which is the so-called photo-voltage and can be used to qualitatively characterize the influence of the photovoltaic effect stemmed from the corrosion products. As shown in Figure 9, the corrosion products of the Cu60-40Zn alloy give rise to positive photo-voltages, and the values are in the range of 7 ~ 28 mV. The positive photo-voltages are caused by the photo-induced holes that flow to the Cu60-40Zn alloy and give it a positive charge (anodic polarization), leaving the photo-generated electrons flowing in the opposite direction to the electrolyte interface, and thus accelerating the cathodic reactions. This kind of positive photo-induced voltages was also detected on Al [61] and weathering steel [62] under UV or visible light illumination, which accelerated the anodic reaction and therefore promoted atmospheric corrosion. These results are consistent with those from this study.

The corrosion products with semiconductor properties on the surface of metal will generate the photoinduced electrons and holes due to the photovoltaic effect under light illumination. The flowing direction of photoinduced electrons determines the promotion or inhibition of corrosion owing to the cathodic/anodic polarization effect aroused by them. Consequently, the flowing direction of electrons and the variations of the galvanic current between the corrosion products and the metal substrate are of significance to elucidate the mechanism of light illumination on the atmospheric corrosion of metals. In this study, the corrosion products derived from 1, 2 and 4 weeks of exposure under UV illumination were peeled off for preparing the CPTF electrodes since it is difficult to directly acquire the photoinduced current information between the metal substrate and corrosion products on a corroded Cu60-40Zn alloy.

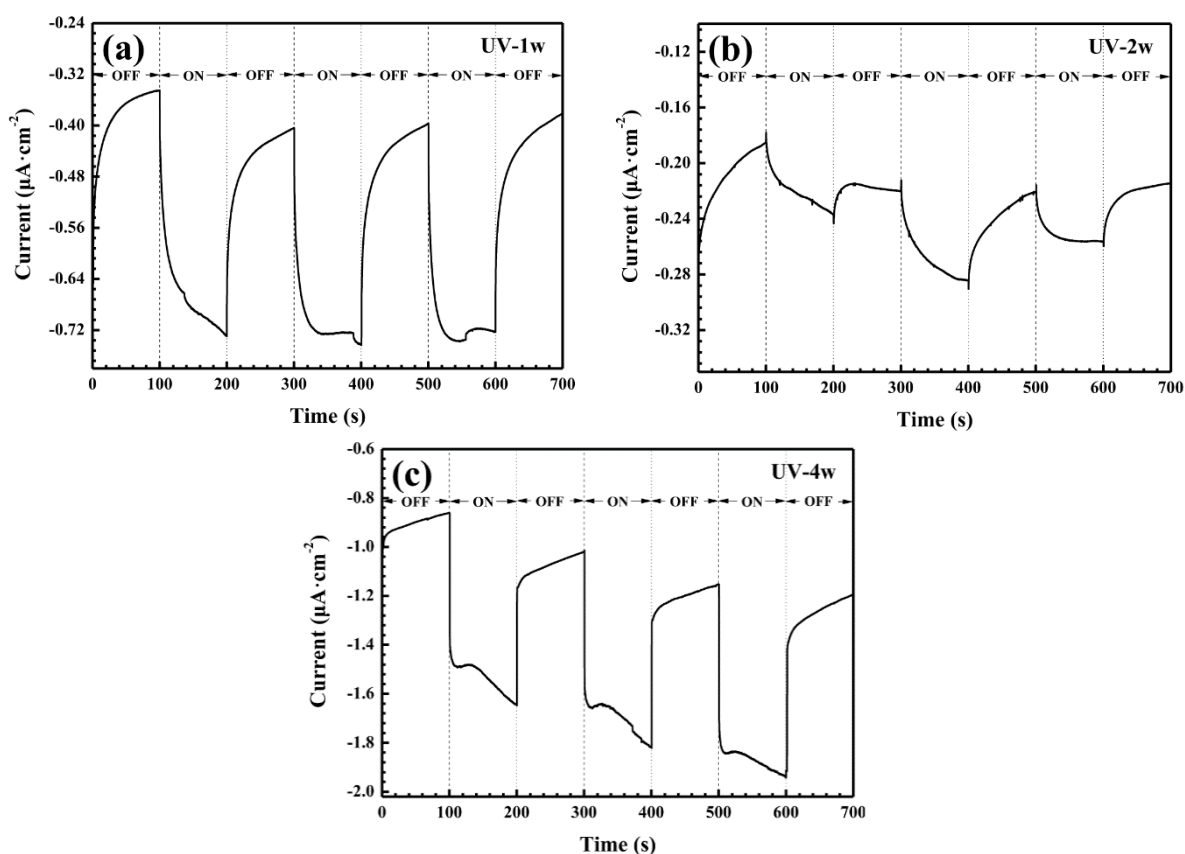


Figure 10. The galvanic current densities between CPTF electrodes and the Cu60-40Zn alloy in 5.2 wt% NaCl solution under intermittent white light illumination. The CPTF electrodes were made from corrosion specimens after 1 (a), 2 (b) and 4 (c) weeks of exposure under UV illumination in humid pure air with 97% RH at 25 °C.

The variations of the galvanic current densities between the CPTF electrodes and the Cu60-40Zn alloy electrode in 5.2 wt% NaCl solution under intermittent white light illumination were measured using the CHI660D Electrochemical Workstation, and the results are presented in Figure 10. All of the stable galvanic currents are negative despite of illumination, manifesting that electrons transfer from the Cu60-40Zn alloy electrode to CPTF electrodes via the potentiostat according to the connection mode in this study. The Cu60-40Zn alloy electrode would serve as the anode (versus CPTE

electrode), which suffers from the anodic dissolution and consequently leads to the acceleration in the cathodic reaction of oxygen reduction. A striking decrease of galvanic current takes place associated with the light illumination, and vice versa, the galvanic current increases remarkably as soon as the white light was switched off. The resulting photoinduced current densities are in the range of -0.05 to $-0.79 \mu\text{A}\cdot\text{cm}^{-2}$. As shown in Figure 10, the galvanic current increased steeply towards the negative direction as soon as the white light was switched on, delivering an instant acceleration in the rate of anodic dissolution of the Cu60-40Zn alloy. This is due to the electrons captured by the photoinduced holes from the Cu60-40Zn alloy electrode under white light illumination. Photoinduced current measurement clearly demonstrates that the photovoltaic effect of the corrosion products formed on the Cu60-40Zn alloy exposed under UV illumination can accelerate the corrosion rate of the Cu60-40Zn alloy substrate, as well as promoting the atmospheric corrosion under UV illumination. This phenomenon was also reported when Cu was exposed under UV illumination in atmospheric environment. The photons interact with the n-type Cu_2O semiconductor and generate extra anodic photocurrent which doubled the corrosion rate of Cu [63]. In addition, Lin et al. found that UV illumination accelerates anodic reaction of Ag because extra anodic photocurrent can be generated and UV generates photoinduced holes in corrosion products which make mass transfer easier for localized corrosion [64].

3.7 Effect of UV illumination on the atmospheric corrosion of the Cu60-40Zn alloy

As the results shown in Figure 2, the atmospheric corrosion of the Cu60-40Zn alloy deposited with NaCl is enhanced by UV illumination. Zhang et al. reported that the β -phase with a higher susceptibility for initial corrosion generally exhibited a lower Volta potential compared with the surrounding α -phase [19]. As the corrosion morphologies of specimens exposed in the dark (Figures 3a-c), the center of the observed area might be the β -phase for corrosion initiation, whereas the surrounding area might be the α -phase that suffered from slight corrosion. The OCPs of the corrosion products formed under UV illumination swiftly shifted to the positive direction (Figure 9), and the photoinduced holes captured the electrons from the Cu60-40Zn alloy (Figure 10) under white light.

Based on the experimental results shown in Figures 10 and 2, the anodic photoinduced current and the increase of the atmospheric corrosion rates of the Cu60-40Zn alloy were observed, demonstrating that the corrosion products mainly embodied the characteristics of n-type semiconductor [63]. Among the atmospheric corrosion products formed on the Cu60-40Zn alloy, Cu_2O , CuO , and ZnO possess semiconductor properties. Typically, ZnO is a wide-bandgap semiconductor and suffers from the doping asymmetry problem, in which the n-type conductivity can be obtained rather easily [20, 58, 59]. Normally, Cu_2O formed in the presence of chloride ions exhibits n-type semiconductor property due to the chloride doping [65]. Therefore, the Cl^- -containing electrolyte in this work may have an effect on the conductivity of corrosion products because the n-type Cu_2O films doped with Cl^- ions exhibited poor protective properties against Cu corrosion [66].

In addition, both the XPS and the FT-IR analyses in this work imply that the UV illumination affects atmospheric corrosion process of the Cu60-40Zn alloy proved by the absence of $\text{Cu}(\text{OH})_2$ in corrosion products. The atmospheric corrosion of a Cu-Zn alloy under NaCl electrolyte film comprises

of the oxidation of Cu and reduction of O₂ [23], according to which the anodic reaction of the Cu60-40Zn alloy could be expressed as:

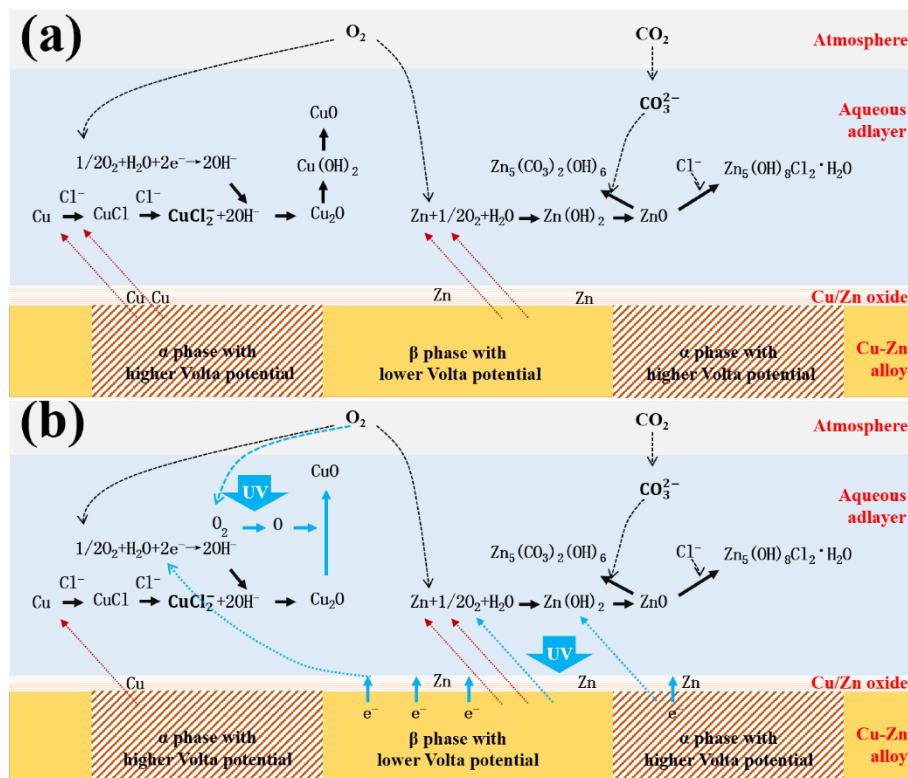


Figure 11. Schematic illustration of the NaCl-induced atmospheric corrosion of the Cu60-40Zn alloy: (a) in the dark; (b) under UV illumination.



and the cathodic reaction :



CuCl could be easily dissolved into NaCl solution, and then form the cuprous complex, i.e., CuCl₂⁻, which would subsequently react with OH⁻ to form Cu₂O on the surface:



The Cu₂O could further transform into Cu(OH)₂ with the increase of exposure time:



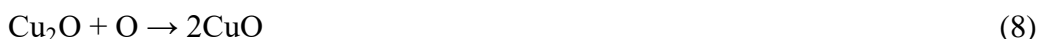
CuO is believed to be the dehydration of Cu(OH)₂ because the former is more stable than the latter [67, 68]:



All these aforementioned reactions were conducted without illumination. Nonetheless, the UV illumination made the corrosion process more sophisticated, e.g., no Cu(OH)₂ was detected in the corrosion products. It has been reported that the molecular oxygen would be disintegrated into two oxygen atoms as long as the wavelength of UV light is shorter than 242 nm [18, 69].

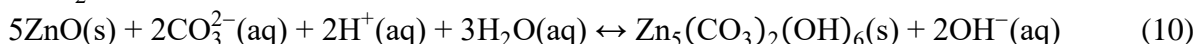


Atomic oxygen is extremely aggressive as previous researches had already proved that atomic oxygen has a stronger acceleration effect than ozone [18, 70, 71]. The aggressive oxygen could react with Cu₂O to produce CuO under UV illumination, which can be expressed as:

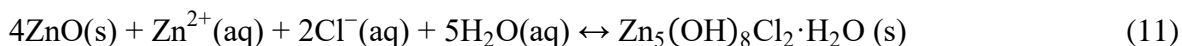


Apart from the acceleration effect of atomic oxygen, the scarcity of Cu²⁺ gives rise to the absence of Cu(OH)₂ in the corrosion products under UV illumination [72]. It has been reported that the Cu(OH)₂ (s) could be formed in near-neutral solution with Cu²⁺ concentration higher than 5×10⁻⁸ M in 10⁻³ M NaCl solution [72]. The respective atomic percentages of Cu in corrosion products under UV illumination derived from XPS are 0.929% and 1.535% with and without sputtering, which are less than 1/10 of that in the dark. Consequently, the relatively low atom percentage of Cu implies the low Cu²⁺ concentration from the anodic reaction of equation (1) under UV illumination, which might lead to the formation of CuO instead of Cu(OH)₂.

In view of the FT-IR analyses and XPS results, the UV illumination has little effect on the constituents of Zn-containing corrosion products, e.g., Zn₅(OH)₈Cl₂·H₂O, Zn₅(CO₃)₂(OH)₆ and ZnO. Corresponding chemical reactions involved in the formation of these constituents were described for the corrosion process of zinc [41, 44, 73-76]. The major Zn-containing corrosion products in this work are hydrozincite mentioned in the previous FT-IR measurements (Figure 4). During the atmospheric corrosion of the Cu60-40Zn alloy, the anodic dissolution of zinc is balanced by oxygen reduction in the cathodic areas leading to the generation of Zn(OH)₂. Zn(OH)₂ can dehydrate to ZnO and subsequently react with carbonate ions supplied by atmospheric carbon dioxide.



Therefore, the Zn-containing corrosion products would be ZnO, Zn(OH)₂ and hydrozincite (Zn₅(CO₃)₂(OH)₆) in humid air. With the presence of NaCl in the solution, the cations, i.e., Na⁺, will migrate towards the cathodic areas, and meanwhile, the anions, i.e., Cl⁻, will move towards the zinc dissolution sites. Both chloride activities and pH values respectively lead to the formation of ZnO in the cathodic areas, while the simonkolleite (Zn₅(OH)₈Cl₂·H₂O) tends to precipitate close to the anodic sites.



The effect of UV illumination on the atmospheric corrosion for the Cu60-40Zn alloy is schematically depicted in Figure 11. Firstly, oxygen could react with Cu₂O to produce CuO under UV illumination. Furthermore, these aggressive oxygen atoms also might accelerate the formation of ZnO, and thus promotes the dezincification of Cu60-40Zn alloy. Secondly, the photo-induced holes generated from the photoelectrochemical effect of n-type corrosion products under UV illumination lead to the positive photo-voltages and therefore promote the anodic dissolution of Cu60-40Zn alloy. This implies that some of the α phases, apart from β phases, could be anodic polarized and suffer from anodic dissolution, which finally results in the promotion of the atmospheric corrosion of the Cu60-40Zn alloy under UV illumination.

4. CONCLUSIONS

The effect of UV illumination on the NaCl-induced atmospheric corrosion of a Cu60-40Zn alloy was studied in a laboratory exposure by microgravimetry, FT-IR spectroscopy, SEM, XPS and electrochemical methods in this paper. The atmospheric corrosion of the Cu60-40Zn alloy pre-deposited with NaCl is promoted by UV illumination. The Zn-containing products mainly comprise of $Zn_5(OH)_8Cl_2 \cdot H_2O$, $Zn_5(CO_3)_2(OH)_6$ and ZnO despite of the UV illumination. $Cu(OH)_2$, CuO, and Cu_2O are formed in the dark, whereas, only CuO and Cu_2O are detected under UV illumination. It is extremely probable that aggressive atomic oxygen can be produced under UV illumination which directly reacts with Cu_2O to produce CuO. In addition, the relatively low atom percentage of Cu in the corrosion film implies low Cu^{2+} concentration, which might lead to the formation of CuO instead of $Cu(OH)_2$. Besides, UV illumination could promote the dezincification of Cu60-40Zn alloy to some extent. UV illumination affects the atmospheric corrosion morphologies of the Cu-Zn alloy. After exposure in the dark, a typical dezincification of meringue deposition on the Cu60-40Zn alloy was observed characterized by central granular crystals surrounded with needle-like crystals; comparatively, more corroded initiation sites presented as porous and whisker islands that distribute dispersively on the surface of the Cu60-40Zn alloy under UV illumination. Corrosion products of the Cu60-40Zn alloy have photoelectric rectifying characteristics similar to n-type semiconductors, which might be associated with ZnO and Cu_2O doped with Cl⁻. A sharp noble shift of OCPs for the n-type corrosion products took place once the white light was on. This was attributed to the photoinduced holes generated from the corrosion products which then captured electrons from the Cu60-40Zn alloy and led to photogenerated electrons flowing from the Cu60-40Zn alloy to the corrosion products. Compared to the typical dezincification in the dark, this photoinduced process directly accelerates the anodic process and furthermore induces more corrosion initiation sites where both the α phase and the β phase might be included under UV illumination, and consequently promotes the atmospheric corrosion of the Cu60-40Zn alloy.

ACKNOWLEDGEMENTS

This work was financially supported by the National Natural Science Foundation of China (No.41576114), Qingdao Innovative Leading Talent Foundation (NO.15-10-3-15-(39)-zch), and Qingdao Science and Technology Achievement Transformation Guidance Plan (NO.14-2-4-4-jch). And this work was also financially supported by State Key Laboratory for Marine Corrosion and Protection, Luoyang Ship Material Research Institute, China (No.614290101011703, KF160402 and KF160413).

References

1. J. Davis, ASM Specialty Handbook: Copper and Copper Alloys, *United States of America: ASM International*, USA, 2001, 652.
2. W.I. Odnevall, X. Zhang, S. Goidanich, B.N. Le, G. Herting, C. Leygraf, *Sci. Total Environ.*, 472 (2014) 681.
3. G. Kammlott, J. Franey, T. Graedel, *J. Electrochem. Soc.*, 131 (1984) 505.
4. G.A. El-Mahdy, A.K.F. Dyab, A.M. Atta, H.A. Al-Lohedan, *Int. J. Electrochem. Sci.*, 8 (2013)

- 9858.
5. A. Kawashima, A. Agrawal, R. Staehle, Effect of oxyanions and chloride ion on the stress corrosion cracking susceptibility of admiralty brass in nonammoniacal aqueous solutions, *ASTM International*, 1979.
 6. M.I. Abbas, *Br. Corros. J.*, 26 (2013) 273.
 7. A. Taylor, *J. Electrochem. Soc.*, 118 (1971) 854.
 8. S. Goidanich, J. Brunk, G. Herting, M.A. Arenas, I.O. Wallinder, *Sci. Total Environ.*, s 412–413 (2011) 46.
 9. E. Sarver, Y. Zhang, M. Edwards, *Corros. Rev.*, 28 (2010) 155.
 10. K.R. Trethewey, I. Pinwill, *Surf. Coat. Technol.*, 30 (1987) 289.
 11. A.A.E. Warraky, *Br. Corros. J.*, 32 (2013) 57.
 12. R. Herman, A. Castillo, *Astm Special Technical Publication*, (1974).
 13. T.L. Barr, J.J. Hackenberg, *Appl. Surf. Sci.*, 10 (1982) 523.
 14. M. Forslund, C. Leygraf, C.J. Lin, J.S. Pan, *Corrosion*, 69 (2013) 468.
 15. C. Leygraf, I.O. Wallinder, J. Tidblad, T. Graedel, Atmospheric corrosion, *John Wiley & Sons*, (2016).
 16. J. Ninlachart, K.S. Raja, *Meeting Abstracts*, MA2018-01 (2018) 1046.
 17. L. Huang, G.S. Frankel, *J. Electrochem. Soc.*, 160 (2013) C336.
 18. Z. Chen, D. Liang, G. Ma, G. Frankel, H. Allen, R. Kelly, *Corros. Eng.Sci.Techn*, 45 (2010) 169.
 19. X. Zhang, X. Liu, I.O. Wallinder, C. Leygraf, *Corros. Sci.*, 103 (2016) 20.
 20. S. Maroie, G. Haemers, J.J. Verbist, *Appl. Surf. Sci.*, 17 (1984) 463.
 21. O. Madelung, Semiconductors: Data Handbook, *Springer Berlin Heidelberg*, (2004).
 22. S.M. Wilhelm, Y. Tanizawa, C.-Y. Liu, N. Hackerman, *Corros. Sci.*, 22 (1982) 791.
 23. Y. Zhang, Z. Xiao, Y. Zhao, Z. Li, Y. Xing, K. Zhou, *Mater. Chem. Phys.*, (2017) 54.
 24. J.N. Nian, C.C. Tsai, P.C. Lin, H. Teng, *J. Electrochem. Soc.*, 156 (2009) S163.
 25. A. Nazarov, E. Diler, P. Dan, D. Thierry, *J. Electroanal. Chem.*, 737 (2015) 129.
 26. A.T. Marin, D. Muñoz-Rojas, D.C. Iza, T. Gershon, K.P. Musselman, J.L. Macmanus-Driscoll, *Adv. Funct. Mater.*, 23 (2013) 3413.
 27. G. Pantazopoulos, A. Vazdirvanidis, *Micos. Micr.*, (2008) 13.
 28. J. Dutkiewicz, F. Masdeu, P. Malczewski, A. Kukula, *Archives of Materials Science & Engineering*, 39 (2009) 80.
 29. Z.Y. Chen, S. Zakipour, D. Persson, C. Leygraf, *Corrosion*, 60 (2004) 479.
 30. L. Song, Z. Chen, *Corros. Sci.*, 86 (2014) 318.
 31. ISO, International Organization for Standardization, 2009.
 32. S. Chu, Y. Wang, Y. Guo, J. Feng, C. Wang, W. Luo, X. Fan, Z. Zou, *Acs Catalysis*, 3 (2013) 912.
 33. J. Xu, L. Zhang, R. Shi, Y. Zhu, *J. Mater. Chem. A*, 1 (2013) 14766.
 34. Z. Chen, F. Cui, R. Kelly, *J. Electrochem. Soc.*, 155 (2008) C360.
 35. L. Song, Z. Chen, *J. Electrochem. Soc.*, 162 (2014) C79.
 36. L. Song, X. Ma, Z. Chen, B. Hou, *Corros. Sci.*, 87 (2014) 427.
 37. L. Song, Z. Chen, B. Hou, *Corros. Sci.*, 93 (2015) 191.
 38. D. Landolt, Introduction to surface reactions: Electrochemical basis of corrosion, *Marcel Dekker, Inc*, USA, 1995, 1.
 39. I. Cole, T. Muster, S. Furman, N. Wright, A. Bradbury, *J. Electrochem. Soc.*, 155 (2008) C244.
 40. I.S. Cole, T.H. Muster, D. Lau, N. Wright, N.S. Azmat, *J. Electrochem. Soc.*, 157 (2010) C213.
 41. I. Odnevall, C. Leygraf, *Corros. Sci.*, 34 (1993) 1213.
 42. S. Song, Z. Chen, *J. Electrochem. Soc.*, 161 (2014) C288.
 43. T. Prosek, A. Nazarov, U. Bexell, D. Thierry, J. Serak, *Corros. Sci.*, 50 (2008) 2216.
 44. E. Diler, B. Rouvellou, S. Rioual, B. Lescop, G. Nguyen Vien, D. Thierry, *Corros. Sci.*, 87

- (2014) 111.
45. A.K. Neufeld, I.S. Cole, *Corrosion*, 53 (1997) 788.
 46. O.K. Srivastava, E.A. Secco, *Can. J. Chem.*, 45 (1967) 585.
 47. G. Poling, *J. Electrochem. Soc.*, 116 (1969) 958.
 48. M. Apos, Keeffe, *J. Chem. Phys.*, 39 (1963) 1789.
 49. T. Minoru, *Bull. Chem. Soc. Jpn.*, 37 (1964) 766.
 50. R.A. Nyquist, R.O. Kagel, *Infrared spectra of inorganic compounds*, *ACADEMIC*, (1971).
 51. L. Zhang, W. Lu, Y. Feng, J. Ni, L. Yong, X. Shang, *Acta Physico Chimica Sinica*, 24 (2008) 2257.
 52. L.M. Peter, D. Vanmaekelbergh, Time and frequency resolved studies of photoelectrochemical kinetics, *Advances in Electrochemical Science and Engineering*, (1999).
 53. J. Duchoslav, M. Arndt, T. Keppert, G. Luckeneder, D. Stifter, *Anal. Bioanal. Chem.*, 405 (2013) 7133.
 54. L.S. Dake, D.R. Baer, J.M. Zachara, *Surf. Interface Anal.*, 14 (1989) 71.
 55. G. Deroubaix, P. Marcus, *Surf. Interface Anal.*, 18 (1992) 39.
 56. N.S. McIntyre, M.G. Cook, *Anal. Chem.*, 47 (1975) 2208.
 57. A.I. Stadnichenko, A.M. Sorokin, A.I. Boronin, *J. Struct. Chem.*, 49 (2008) 341.
 58. D.C. Look, B. Claflin, *Physica Status Solidi*, 241 (2004) 624.
 59. V. Avrutin, D.J. Silversmith, H. Morkoc, *Proceedings of the IEEE*, 98 (2010) 1269.
 60. H. Lin, G. Frankel, *J. Electrochem. Soc.*, (2013) C336.
 61. T.D. Burleigh, C.D. Ruhe, J.D. Forsyth, *Corrosion Houston Tx*, 59 (2003) 366.
 62. P. Qiu, *Int. J. Electrochem. Sci*, 11 (2016) 10498.
 63. H. Lin, G. Frankel, *Corros. Eng.Sci.Techn*, 48 (2013) 461.
 64. H. Lin, G.S. Frankel, *Corrosion*, 69 (2013) 1060.
 65. X. Han, K. Han, T. Meng, *Electrochem. Solid-State Lett.*, 12 (2009) H89.
 66. A.D. Modestov, G.D. Zhou, H.H. Ge, B.H. Loo, *J. Electroanal. Chem.*, 380 (1995) 63.
 67. V. Chalyi, *Russ. J. Inorg. Chem.*, 8 (1963) 269.
 68. M. Ugorets, E. Buketov, K. Akhmetov, *Russian Jour. Inorganic Chem*, 13 (1968) 1525.
 69. B.J. Finlayson Pitts, J.N. Pitts Jr, *Chemistry of the upper and lower atmosphere: theory, experiments, and applications*, *Academic press*, (1999).
 70. D. Liang, H. Allen, G. Frankel, Z. Chen, R. Kelly, Y. Wu, B. Wyslouzil, *J. Electrochem. Soc.*, 157 (2010) C146.
 71. Y. Wan, E.N. Macha, R.G. Kelly, *Corrosion Houston Tx*, 68 (2012) 036001.
 72. J. Vuceta, J.J. Morgan, *Limnol. Oceanogr.*, 22 (1977) 742.
 73. T. Graedel, *J. Electrochem. Soc.*, 136 (1989) 193C.
 74. J. Svensson, L. Johansson, *Corros. Sci.*, 34 (1993) 721.
 75. I. Odnevall, C. Leygraf, *Corros. Sci.*, 36 (1994) 1551.
 76. Q. Qu, C. Yan, Y. Wan, C. Cao, *Corros. Sci.*, 44 (2002) 2789.